Carbon defects as sources of the green and yellow luminescence bands in undoped GaN

M. A. Reshchikov* and D. O. Demchenko
Department of Physics, Virginia Commonwealth University, Richmond, Virginia 23284, USA

A. Usikov
Nitride Crystals, Inc., 181 East Industry Court, Suite B, Deer Park, New York 11729, USA
and Saint-Petersburg National Research University of Information Technologies, Mechanics and Optics, Saint Petersburg, 197101, Russian Federation

H. Helava and Yu. Makarov
Nitride Crystals, Inc., 181 East Industry Court, Suite B, Deer Park, New York 11729, USA
(Received 30 June 2014; revised manuscript received 4 November 2014; published 12 December 2014)

In high-purity GaN grown by hydride vapor phase epitaxy, the commonly observed yellow luminescence (YL) band gives way to a green luminescence (GL) band at high excitation intensity. We propose that the GL band with a maximum at 2.4 eV is caused by transitions of electrons from the conduction band to the $0/+$ level of the isolated C_N defect. The YL band, related to transitions via the $-/0$ level of the same defect, has a maximum at 2.1 eV and can be observed only for some high-purity samples. However, in less pure GaN samples, where no GL band is observed, another YL band with a maximum at 2.2 eV dominates the photoluminescence spectrum. The latter is attributed to the C_NO_N complex.

DOI: 10.1103/PhysRevB.90.235203 PACS number(s): 78.55.Cr, 71.55.Eq, 61.72.uj, 71.15.Mb

I. INTRODUCTION

Gallium nitride (GaN) is a promising material for high-power/high-frequency electronics [1–4]. In particular, thick GaN layers on sapphire substrates and freestanding GaN, grown by hydride vapor phase epitaxy (HVPE), are expected to have very high breakdown voltage due to a low density of defects in this material. In photoluminescence (PL) studies of high-quality freestanding GaN grown by HVPE, the yellow luminescence (YL) band with a maximum at about 2.2 eV and the green luminescence (GL) band with a maximum at about 2.4 eV are the dominant defect-related PL bands [5]. Previously, the YL and GL bands were attributed to transitions of electrons from the conduction band to the $2-/-$ and $-/0$ transition levels, respectively, of the gallium vacancy-oxygen ($V_{Ga}O_N$) complex [6]. However, according to recent calculations using hybrid functionals, the PL band caused by transitions of electrons from the conduction band to the $2-/-$ level of $V_{Ga}O_N$ is expected to have a maximum at 1.4 eV; i.e., in the infrared region [7]. Moreover, the exponential decay of the GL band at low temperatures was explained with the assumption that the GL band is caused by transitions of electrons from an excited state, located very close to the conduction band minimum (CBM), to the $-/0$ level of the $V_{Ga}O_N$ acceptor [5]. However, such an assumption is not well justified. Indeed, an excited state close to the conduction band is possible for a positively charged deep donor, whereas the $V_{Ga}O_N$ acceptor does not have donorlike excited states. Thus, a revision of the attribution for the GL band in GaN is needed.

Regarding the YL band, two assignments have been recently suggested based on modern first-principles calculations. Lyons *et al.* [8] attributed the YL band to the C_N defect, whereas Demchenko *et al.* [7] proposed that the YL band is caused by the C_NO_N complex. The C_NO_N complex is a deep donor with the $0/+$ level at 0.75 eV above the valence band maximum (VBM). The C_N defect in GaN is a deep acceptor with the $-/0$ level at 0.9–1.1 eV above the VBM [7,8]. The schematic band diagram, including these thermodynamic transition levels, is shown in Fig. 1.

In addition to the acceptor $-/0$ level of C_N, calculations have predicted the existence of the $0/+$ level for this defect at 0.43 eV above the VBM [7]. Since the $-/0$ level of C_N and the $0/+$ level of C_NO_N have similar energies, it is possible that both the C_N and C_NO_N defects produce YL bands with similar shapes and positions (Fig. 1). However, due to the difference in their electronic structure, these defects can be distinguished through the study of the effect of excitation intensity on the PL spectrum. Indeed, it is expected that the C_N acceptors in *n*-type GaN can be saturated with holes (causing saturation of the YL band intensity), and at higher excitation intensities the defects will begin to capture an additional hole. Subsequently, transitions of electrons from the conduction band to the $0/+$ level of C_N will cause a "secondary" PL band, which peaks at higher photon energies (Fig. 1). Lyons *et al.* [9] calculated that optical transitions of electrons from the conduction band to this level would cause a *blue* band with a maximum at about 2.7 eV. These authors noticed that in C-doped GaN, a blue band is often observed when the carbon concentration is high [10,11], or at high excitation intensity [12,13], which, in their opinion, supported the existence of the $0/+$ level of the C_N defect. In contrast, there is only one optically active transition level for the C_NO_N complex in the band gap of GaN. A second level, $+/2+$ is predicted to be very close to the valence band (Fig. 1) and will act as a repulsive center for holes. Therefore, the saturation of the C_NO_N-related YL band will not be followed by the emergence of another PL band

*mreshchi@vcu.edu

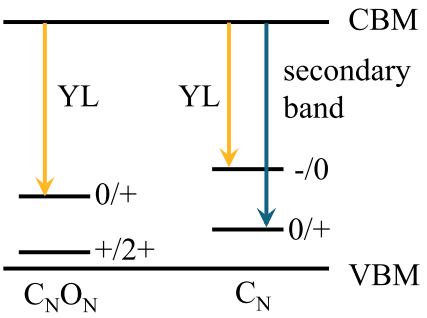

FIG. 1. (Color online) Schematic band diagram and predicted transition levels for the C_NO_N complex and the isolated C_N defect. Calculations predict that the C_NO_N complex forms the $0/+$ transition level in the band gap, while C_N forms two transition levels: $(-/0$ and $0/+$. The C_NO_N complex is expected to generate only the YL band. The C_N defect can generate the YL band and an additional, higher energy band after the YL is saturated.

at higher photon energies. This important distinction between the two defects should allow reliable attribution of the YL band to either C_N or C_NO_N, depending on the existence of the secondary band.

In this paper, we investigated the PL behavior for a number of GaN samples. We arrived at the conclusion that the GL band with a maximum at 2.4 eV, and not the blue band, is caused by electron transitions via the $0/+$ level of the C_N defect. The PL bands associated with the C_N and C_NO_N defects can both be called YL bands since they have only slightly different positions of their maxima. It appears that in a majority of GaN samples, the C_NO_N complex is responsible for the YL band. The C_N defect can be revealed through the observation of the secondary (GL) band only in high-quality GaN grown by the HVPE technique. In this paper, time-resolved PL experiments have been employed to identify the GL band due to its short lifetime and exponential decay even at low temperatures (30–100 K).

II. METHODS

A. Experimental details

We observed the GL band (at least in time-resolved PL measurements) in more than 20 samples, which were 10- to 30-μm-thick unintentionally doped GaN layers grown by HVPE on c plane, 2 in. sapphire substrates. The growth was performed at temperatures of 850–1000 °C, in atmospheric pressure and in an argon ambient. Ammonia and HCl were used as the precursors. The growth rate (0.2–1 μm/min) was controlled by the HCl gas flow rate through the Ga source. For a more detailed study, two representative samples were selected: 1007 and RS280. The concentration of free electrons, n, given in Table I for these two samples, is calculated from the PL lifetime of the YL band at room temperature, according to a model presented in Ref. [14], while the direct Hall effect measurements showed an apparent concentration of about three times higher due to the existence of a highly conductive layer near the GaN/sapphire interface [15].

An additional HVPE-grown sample in this paper was undoped freestanding GaN produced at the Samsung Advanced Institute of Technology (sample B73). The HVPE samples were compared to GaN samples grown by metal-organic chemical vapor deposition (MOCVD) on sapphire substrates, in which no traces of the GL band could be found (samples EM1256, EM6881, EM7169, and EM7049) [16,17].

The concentration of C and O impurities ([C] and [O], respectively) were estimated from secondary ion mass-spectrometry (SIMS) measurements and are given in Table I. The carbon concentration in the MOCVD-grown samples was varied in the range of $[C] = 4 \times 10^{16} - 2 \times 10^{17}\,cm^{-3}$ by changing growth conditions. Samples EM6881, EM7169, and EM7049 are semi-insulating, and only the lower bound for their resistivity can be estimated.

Steady-state PL was excited with an unfocused He-Cd laser (50 mW, 325 nm), dispersed by a 1200 rules/mm grating in a 0.3 m monochromator and detected by a cooled photomultiplier tube. Calibrated neutral-density filters were used to attenuate the excitation power density (P_{exc}) over the range 10^{-5}–$0.2\,W/cm^2$, while a focused beam with a diameter of 0.2 mm was used to obtain P_{exc} up to $100\,W/cm^2$. Time-resolved PL was excited with a nitrogen pulse laser (1 ns pulses, with a repetition rate of 6 Hz, and 337 nm wavelength). The excitation light intensity at the sample surface, P_0, was varied between 10^{18} and $10^{24}\,cm^{-2}s^{-1}$ using neutral density filters. A closed-cycle optical cryostat was used for temperatures between 15 and 320 K. The absolute internal quantum efficiency of PL η is defined as $\eta = I^{PL}/G$, where I^{PL} is the integrated PL intensity from a particular PL band and G is the concentration of electron-hole pairs created by the laser per second in the same volume. To find η for a particular PL band, we compared its integrated intensity with the PL intensity obtained from a calibrated GaN sample [18,19]. All samples were studied under identical conditions.

TABLE I. Parameters of GaN samples analyzed in this paper.

Sample number	Growth method	Thickness (μm)	[C] from SIMS (cm^{-3})	[O] from SIMS (cm^{-3})	n at 300 K (cm^{-3})	ρ at 300 K (Ωcm)
1007	HVPE	22	7×10^{16}	1×10^{17}	6×10^{16}	~0.1
RS280	HVPE	27	0.5×10^{16}	6×10^{16}	2×10^{16}	~0.1
B73	HVPE	200	$\sim 1 \times 10^{16}$	$\sim 2 \times 10^{16}$	1.3×10^{16}	0.4
EM1256	MOCVD	2.2	4×10^{16}	5×10^{16}	2×10^{16}	0.6
EM6881	MOCVD	3.2	7×10^{16}	5×10^{16}	–	$>10^{11}$
EM7169	MOCVD	2.5	1×10^{17}	6×10^{16}	–	$>10^{11}$
EM7049	MOCVD	1.9	2×10^{17}	5×10^{16}	–	$>10^{11}$

B. Theoretical details

To find the transition levels for the C_N and C_NO_N defects, we performed Heyd-Scuseria-Ernzerhof (HSE) hybrid functional [20] calculations. As in a previous paper [7], we adjusted the fraction of exact exchange to 0.312 and the screening parameter to 0.2 Å^{-1}. The computed band gap of 3.50 eV agrees with the low-temperature experimental value of 3.50 eV, and the computed relaxed lattice parameters for wurtzite GaN ($a = 3.210$ Å, $c = 5.198$ Å, and $u = 0.377$) also agree with the experimental values ($a = 3.189$ Å and $c = 5.185$ Å) [21]. The 128 atom supercells were used with all internal degrees of freedom relaxed using HSE hybrid functional calculations to result in forces of 0.05 eV/Å or less. The plane-wave basis sets with a 400 eV cutoff at the Γ point were used in all calculations. Spin-polarized calculations were performed in all cases. The details of the calculation methods and corrections to defect energies can be found in Ref. [7].

It is necessary to mention a practical issue regarding the potential alignment ΔV correction, which originates from dropping the diverging $\mathbf{G} = 0$ term in the Fourier energy expansion in a charged supercell [22]. This correction is relatively small (0.05 to 0.1 eV) and is proportional to the defect charge. In this paper, we compared the results of calculations with experimental measurements and analyzed the effect this correction has on the computed properties of different types of defects (e.g., isolated defects vs complexes). Although there are no significant changes to the final results, it appears that the potential alignment corrections slightly worsen the results for the isolated defect C_N, but slightly improve the results for C_NO_N complex. This may indicate that isolated defects and defect complexes have different electric dipole properties. Therefore, different corrections accounting for the artificial dipole interactions in periodic supercells may have to be applied for the two types of defects. In this study, ΔV was applied only to the C_NO_N complex, which improved the results by up to 0.1 eV. Further study is needed to clarify this behavior.

III. RESULTS

A. Yellow and blue luminescence bands in GaN grown by MOCVD

The YL band in GaN grown by MOCVD has a maximum at 2.2 eV (Figs. 2 and 3). In conductive n-type GaN (sample EM1256), the YL band intensity begins to saturate at excitation intensities $P_{exc} > 10^{-5}$ W/cm^2 (Fig. 2). The shape of the YL band $I^{PL}(\hbar\omega)$ and position of its maximum $\hbar\omega_{max}$ remained unchanged for excitation intensities up to 0.2 W/cm^2. The shape of the YL band at low temperature can be modeled with the following formula derived from a one-dimensional configuration coordinate model [23]

$$I^{PL}(\hbar\omega) \propto \exp\left[-2S_e\left(\sqrt{\frac{E_0 + 0.5\hbar\Omega - \hbar\omega}{E_0 + 0.5\hbar\Omega - \hbar\omega_{max}}} - 1\right)^2\right], \quad (1)$$

where S_e and $\hbar\Omega$ are the Huang-Rhys factor and the dominant phonon energy for the excited state, $\hbar\omega$ is the photon energy, and E_0 is the zero-phonon line (ZPL) energy. The values of $\hbar\Omega$, E_0, and $\hbar\omega_{max}$ (52 meV, 2.64 eV, and 2.20 eV, respectively) are typical for the YL band in GaN [5]. Note that no other luminescence bands can be found in the range from 2.6 to 3.2 eV for the sample with a low concentration of carbon (Fig. 2).

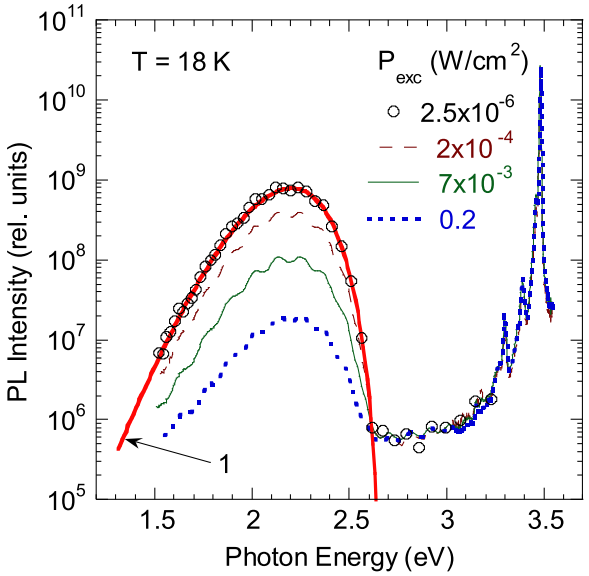

FIG. 2. (Color online) Low-temperature PL spectra from conductive n-type GaN grown by MOCVD (sample EM1256). The PL intensity is divided by the excitation intensity. The thick solid line 1 is calculated using Eq. (1) with the following parameters: $S_e = 7.4$; $E_0 = 2.64$ eV; $\hbar\omega_{max} = 2.20$ eV; and $\hbar\Omega = 52$ meV.

For semi-insulating GaN, a broad band can be found in the blue spectral region only in some samples (Fig. 3) [16]. The band has a maximum at 3.03 eV and is identified as the BL2 band, sometimes observed in high-resistivity GaN grown by MOCVD [24,25]. It has a characteristic fine structure, with the ZPL at 3.333 eV (inset in Fig. 3). In the past, the BL2

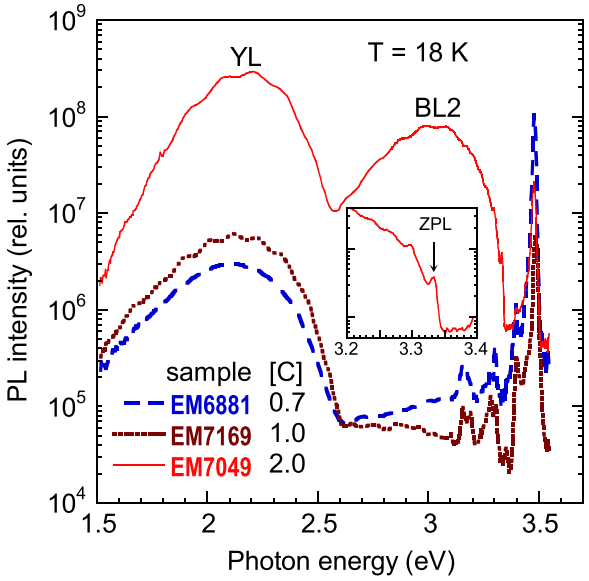

FIG. 3. (Color online) Low-temperature PL spectra at $P_{exc} = 10^{-4}$ W/cm^2 from semi-insulating GaN samples grown by MOCVD. The PL intensity is divided by the excitation intensity. The concentration of carbon [C] is given in units of 10^{17} cm^{-3}. The inset shows a high resolution of the region near the ZPL of the BL2 band.

band has been attributed to transitions of electrons from the conduction band (or from a state very close to the conduction band) to a defect level located at 0.15 eV above the VBM [24]. An important feature of the BL2 band is that it bleaches during continuous ultraviolet (UV) illumination, indicating unstable behavior [25]. It was suggested previously that the BL2 band is associated with some defect complex containing hydrogen, and the bleaching is caused by dissociation of this complex under UV exposure [5,25]. It is unclear why the BL2 band is present only in some semi-insulating GaN samples and cannot be found in others (Fig. 3) and why the YL intensity varies considerably in different samples. Further studies are needed to clarify this issue.

Another blue band (labeled BL) peaking at 2.9 eV (not shown here), which is related to the Zn_{Ga} acceptor, can be observed in semi-insulating GaN, when the BL2 band is quenched and disappears at temperatures above 150 K [25]. Both the BL and BL2 bands apparently have no relation to the isolated C_N defect. On the other hand, the GL band with a maximum at 2.4 eV is a good candidate for transitions via the $0/+$ level of the C_N defect, as will be discussed below.

B. Green luminescence band in freestanding GaN

1. Shape of the GL band

The GL band with a maximum at about 2.4 eV appears under high excitation intensity in the steady-state PL spectrum of high-quality GaN samples grown by the HVPE method. The nearly quadratic dependence of the GL intensity on P_{exc} in n-type GaN is a strong indication that the defect responsible for this band captures two holes before any radiative recombination takes place [6]. However, it is often difficult to resolve the GL band in steady-state PL spectra, because it usually overlaps with the YL band at room temperature and with the UV luminescence (UVL) band or BL band at low temperatures. In this paper, we extracted the shape of the GL band from time-resolved PL measurements, because in these experiments the GL band can be isolated due to its PL lifetime being significantly shorter than that for other defect-related PL bands [26]. Figure 4 shows the PL spectrum taken 1 μs after pulsed excitation at various temperatures. The GL band has a maximum at 2.40 eV and a full width at half-maximum (FWHM) of 0.43 eV at low temperatures. For a very wide range of PL intensities (almost three orders of magnitude), the shape of the GL band can be fit with Eq. (1), as shown in Fig. 4. The PL band shape remains unchanged for different excitation intensities and for different time delays.

At temperatures below 100 K, the shape of the GL band is asymmetric, as is typically observed for defects with moderate electron-phonon coupling. By employing a one-dimensional configuration-coordinate model [5,27], we have estimated the energy of the dominant phonon mode in the excited state as $\hbar\Omega = 41 \pm 5$ meV from the analysis of the temperature dependence of the GL band FWHM as the temperature was increased from 30 to 300 K. Other parameters in Eq. (1) for the GL band were estimated as $S_e = 8.5$, $E_0 = 2.9$ eV, and $\hbar\omega_{max} = 2.4$ eV from the best fit with the experimental data at $T = 30$ and 100 K (Fig. 4). The above-determined parameters, which describe the shapes and positions of the YL and GL bands, will be used in the following sections to simulate the shapes of the YL and GL bands and to resolve them in those PL spectra where they overlap with each other and other PL bands.

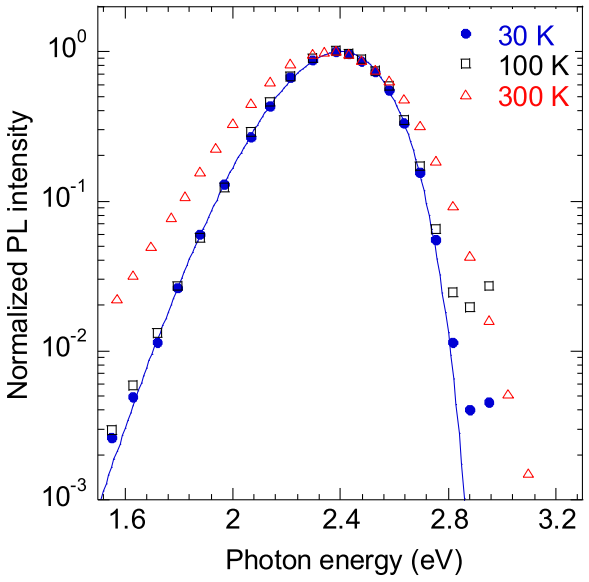

FIG. 4. (Color online) Normalized PL spectra at 10^{-6} s after a laser pulse with $P_0 = 5 \times 10^{23}$ cm^{-2}s^{-1} from freestanding GaN (sample B73). The symbols are experimental points, and the solid curve is calculated using Eq. (1) with the following parameters: $S_e = 8.5$; $E_0 = 2.9$; $\hbar\omega_{max} = 2.4$ eV; and $\hbar\Omega = 41$ meV.

2. Effect of temperature

While the PL from freestanding GaN containing the GL band has been previously studied at temperatures below 300 K [5], we are not aware of any reports on its behavior for higher temperatures. Figure 5 shows the PL spectra from sample B73 for select temperatures. At 300 K, a broad band with a maximum at 2.37 eV consists of two overlapping YL and

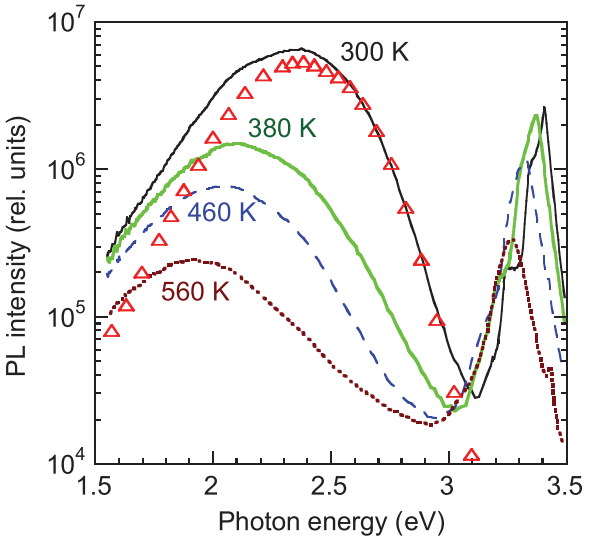

FIG. 5. (Color online) PL spectra at selected temperatures for sample B73. The lines show steady-state PL spectra at $P_{exc} = 0.3$ W/cm^2. Triangles show time-resolved PL spectrum measured at 300 K.

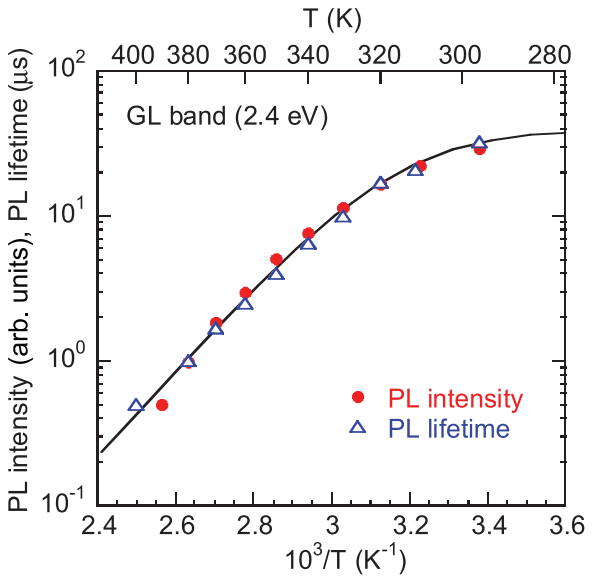

FIG. 6. (Color online) Temperature dependence of the GL band intensity and the GL lifetime for sample B73. The solid line is calculated using Eq. (2) for PL intensity and Eq. (3) for PL lifetime with the following parameters: $\eta_0 = 0.1$; $C_p = 10^{-6}\,\mathrm{cm}^3/\mathrm{s}$; $\tau_0 = 40\,\mu\mathrm{s}$; $E_A = 535\,\mathrm{meV}$; $N_v = 3.2 \times 10^{15}\,T^{3/2}\,\mathrm{cm}^{-3}$; and $g = 2$.

GL bands. The comparison of the steady-state PL spectrum with the time-resolved PL spectrum for the GL band (shown with triangles in Fig. 5) indicates that the contribution from the YL band in the steady-state PL spectrum is small at 300 K (the YL band is not present in the time-resolved PL spectrum due to its long lifetime). The deconvolution of the broad band into the YL and GL bands with known shapes (not shown in Fig. 5) indicates that, as the temperature is increased from 300 to 380 K, the YL band intensity is nearly constant, whereas the intensity of the GL band decreases and it finally disappears at $T \approx 400\,\mathrm{K}$. At temperatures between 380 and 560 K, the defect-related PL band maximum gradually shifts from 2.10 to 1.93 eV. It is not clear whether the broad, red-yellow band consists of two bands associated with two different defects, or if the band is related to a single defect and the band redshifts due to the decreasing band gap with increasing temperature. The near-band-edge (NBE) peak shifts from 3.37 to 3.27 eV as the temperature is increased from 380 to 560 K.

The temperature dependences of the GL band intensity and the GL lifetime are shown in Fig. 6. The dependences are very similar to each other and can be fit with the following expressions [14]

$$I^{\mathrm{PL}}(T) = \frac{I_0}{1 + (1-\eta_0)\tau_0 C_p N_v g^{-1} \exp(-E_A/kT)}, \quad (2)$$

$$\tau(T) = \frac{\tau_0}{1 + (1-\eta_0)\tau_0 C_p N_v g^{-1} \exp(-E_A/kT)}, \quad (3)$$

where I_0, η_0, and τ_0 are the PL intensity, quantum efficiency, and PL lifetime, respectively, for the GL band before PL quenching begins (at about 290 K), C_p is the hole-capture coefficient for the defect state responsible for the GL band, N_v is the effective density of states in the valence band, E_A is the energy distance between the VBM and the defect state responsible for the GL band, and g is its degeneracy. From the fit, shown with a solid line in Fig. 6, we have estimated that $E_A \approx 0.54\,\mathrm{eV}$ and $C_p \approx 10^{-6}\,\mathrm{cm}^3/\mathrm{s}$.

C. Yellow and green luminescence bands in GaN layers grown by HVPE

Detailed studies of the effect of excitation intensity on PL were conducted at $T = 100\,\mathrm{K}$. This temperature was chosen because at lower temperatures, the exciton emission is very strong and may contribute as a parasitic signal at photon energies where the defect-related bands were observed. On the other hand, the temperature-induced broadening of the GL band can be ignored at 100 K, as can be seen in Fig. 4. The contribution of the GL band in the PL spectrum and its PL lifetime varied from sample to sample, apparently due to different concentrations of point defects and free electrons in the set of 20 undoped GaN samples (layers on sapphire) grown by HVPE.

Below, the results are presented for two representative samples: a high-purity sample with the strongest GL band (sample RS280) and a less pure sample in which the YL band was stronger and the GL band could be observed only in time-resolved PL measurements (sample 1007). To evaluate the presence of carbon, oxygen, and a few other impurities, dedicated SIMS measurements for samples RS280 and 1007 have been carried out by the Evans Analytical Group. In this analysis, a very low detection limit for carbon was achieved in vacuum by removing carbon adsorbed at the surface. The reduction in surface carbon resulted in less interference (and thus a lower background/detection limit) during the SIMS measurement of the underlying GaN region. The concentrations of selected impurity species in the two samples are given in Table II. The data for the depths between 2 and 4 μm represents the bulk part of the GaN layers. To compare with PL results, we will limit the analysis to the depth range of 100 to 400 nm, because the concentration of photogenerated charge carriers in our PL experiments is negligible beyond 400 nm, while the SIMS data in the first 100 nm can be affected by impurities absorbed at the surface and can be unrealistic.

1. *High-purity GaN (strong GL and weak YL)*

The steady-state PL spectra for selected excitation intensities and $T = 100\,\mathrm{K}$ for sample RS280 are shown in Fig. 7. In the PL spectra, the NBE emission has a main peak at 3.485 eV and is attributed to the annihilation of free excitons. At low excitation intensities, three defect-related PL bands can be resolved: the UVL band with a main peak at 3.30 eV, the Zn-related BL band with a maximum at 2.94 eV, and the red luminescence (RL) band with a maximum at 1.82 eV. The RL band in undoped GaN grown by HVPE is preliminarily attributed to a deep acceptor with an energy level of 1.13 eV above the valence band [28]. With increasing excitation intensity, the relative contribution of the UVL, BL, and RL bands decreases, and the GL band with a maximum at 2.40 eV emerges (Fig. 7). By subtracting the shapes of the RL and BL bands (obtained from the PL spectrum at the lowest excitation intensity) from the PL spectrum measured at $P_{\mathrm{exc}} = 0.2\,\mathrm{W}/\mathrm{cm}^2$, we obtained a shape of a PL band (the dotted curve in Fig. 7) almost identical to the shape of the GL band found

TABLE II. Concentration of impurities (per cubic centimeter) from SIMS measurements.

	RS280		1007		
Impurity	100–400 nm	2–4 μm	100–400 nm	2–4 μm	Detection limit
C	5.6×10^{15}	0.4×10^{15}	8.2×10^{16}	1.5×10^{15}	1×10^{15}
O	6.9×10^{16}	2×10^{16}	1.3×10^{17}	6.8×10^{15}	1×10^{16}
Si	4.9×10^{15}	2.6×10^{15}	2.3×10^{16}	7.6×10^{16}	8×10^{15}
H	1.6×10^{17}	1.3×10^{17}	3.9×10^{17}	1.3×10^{17}	2×10^{17}
Cl	3.9×10^{15}	1.5×10^{16}	1.7×10^{16}	1×10^{17}	1×10^{15}

from the time-resolved PL in freestanding GaN (Fig. 4). By repeating this procedure for different excitation intensities, we obtained the dependence of the GL intensity on the excitation intensity (Fig. 8). We can see that at $P_{exc} < 10^{-3}$ W/cm^2 the GL intensity increases as approximately a square of P_{exc}. This behavior is expected for optical transitions via the lower transition level of C_N (the 0/+ level) for excitation intensities when the higher transition level (the −/0 level) is not yet saturated with holes (the YL intensity increases linearly with P_{exc}) [6], because the probability of capturing two holes by a defect before recombination occurs is proportional to the square of the excitation intensity. Between 10^{-3} and 1 W/cm^2, the GL band intensity increases linearly with P_{exc}, because one hole is already bound to the defect and only one additional hole needs to be captured. The YL band is expected to be saturated under these conditions. Finally, at $P_{exc} > 1$ W/cm^2 the GL band saturates. The saturation of the RL and BL bands begins at much lower excitation intensities (at $P_{exc} > 10^{-3}$ W/cm^2).

The solid lines in Fig. 8 are calculated with the following expression, which is obtained from rate equations [29,30]

$$I^{PL} = \eta P_0 = \frac{N}{\alpha\tau} \ln\left(1 + \frac{\alpha\tau P_0 \eta_0}{N}\right). \quad (4)$$

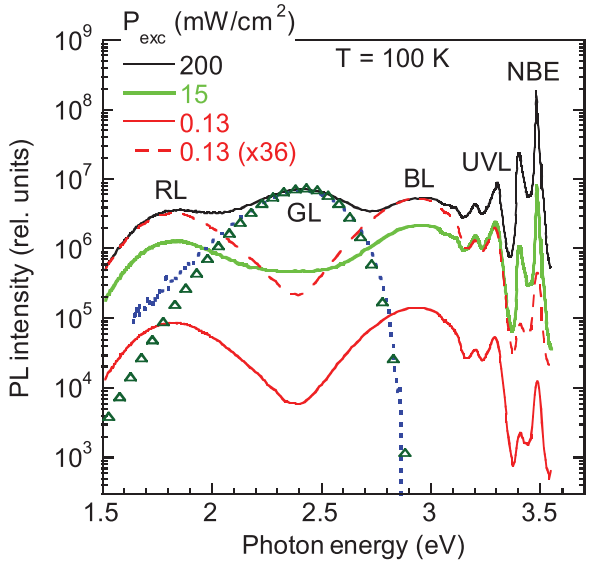

FIG. 7. (Color online) Steady-state PL spectra for sample RS280 at 100 K and selected excitation intensities. The dotted line shows the PL band obtained as a difference between the PL spectrum at 0.13 mW/cm^2 (multiplied by 36) and the PL spectrum at 200 mW/cm^2. Triangles show the shape of the GL band calculated using Eq. (1), with parameters given in Fig. 4.

Here, P_0 is the excitation intensity (expressed as the number of photons passing through a unit area of the sample surface per unit time), N is the concentration of defects responsible for a particular PL band, η_0 is the quantum efficiency of that PL band in the limit of low excitation intensity, and α is the absorption coefficient ($\alpha \approx 1.2 \times 10^5$ cm^{-1} for GaN at 3.81 eV [31]). The only fitting parameter in Eq. (4) is N. From the best fit, we have estimated that the concentrations of defects responsible for the GL, RL, and BL bands are 1.5×10^{15}, 1.5×10^{16}, and 2×10^{15} cm^{-3}, respectively.

The YL band was not observed in the steady-state PL spectra of this sample, because it is obscured by the RL band.

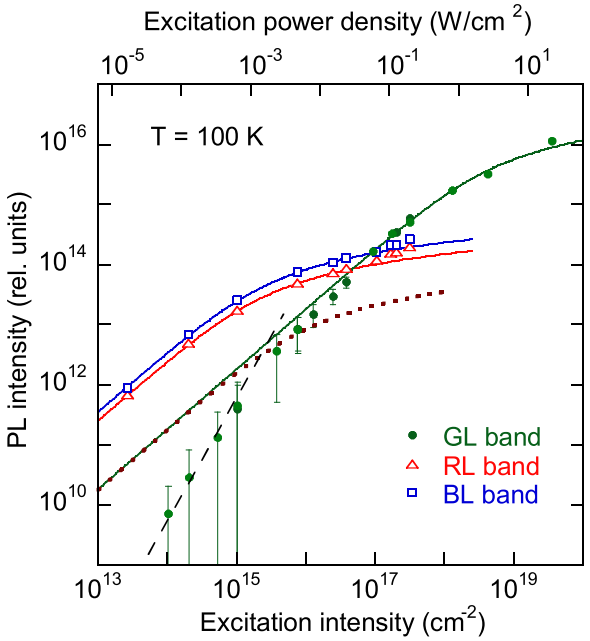

FIG. 8. (Color online) Dependence of the PL intensity on excitation intensity for the major PL bands in steady-state PL measurements for sample RS280 at 100 K. The experimental points for the GL band are obtained from the PL spectra deconvolution similar to an example shown in Fig. 7 but use the PL spectrum at lower excitation intensity of 10^{-5} W/cm^2 as the "background" spectrum. The solid lines are calculated using Eq. (4), with the following parameters: $\eta_0 = 0.0018$; $\tau_0 = 4.5\,\mu$s; and $N = 1.5 \times 10^{15}$ cm^{-3} for the GL band; $\eta_0 = 0.025$; $\tau_0 = 6$ ms; and $N = 1.5 \times 10^{16}$ cm^{-3} for the RL band; and $\eta_0 = 0.035$; $\tau_0 = 500\,\mu$s; and $N = 2 \times 10^{15}$ cm^{-3} for the BL band. The dashed line indicates the quadratic dependence of PL intensity on excitation intensity. The dotted line is calculated using Eq. (4), with $\eta_0 = 0.0018$; $\tau_0 = 2$ ms; and $N = 1.5 \times 10^{15}$ cm^{-3}, which is the expected dependence for the YL band.

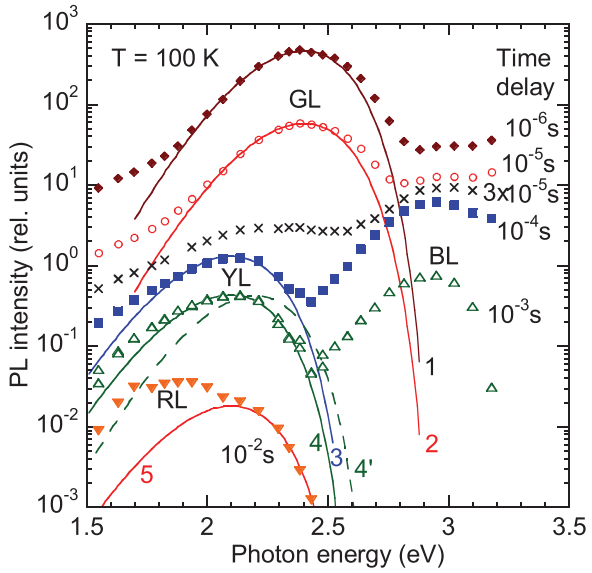

FIG. 9. (Color online) PL spectra at different time delays after pulsed excitation with $P_0 = 5 \times 10^{23}\,\mathrm{cm^{-2}s^{-1}}$ for sample RS280. The symbols are experimental points, and the curves are calculated using Eq. (1), with the following parameters: $S_e = 8.5$; $E_0 = 2.9\,\mathrm{eV}$; $\hbar\omega_{\max} = 2.4$ eV; and $\hbar\Omega = 41$ meV (curves 1 and 2); $S_e = 7.4$; $E_0 = 2.57\,\mathrm{eV}$; $\hbar\omega_{\max} = 2.1$ eV; and $\hbar\Omega = 56$ meV (curves 3, 4, and 5). The dashed curve 4′ corresponds to the YL band shown in Fig. 12, with $S_e = 7.4$; $E_0 = 2.64\,\mathrm{eV}$; $\hbar\omega_{\max} = 2.2$ eV; and $\hbar\Omega = 56$ meV.

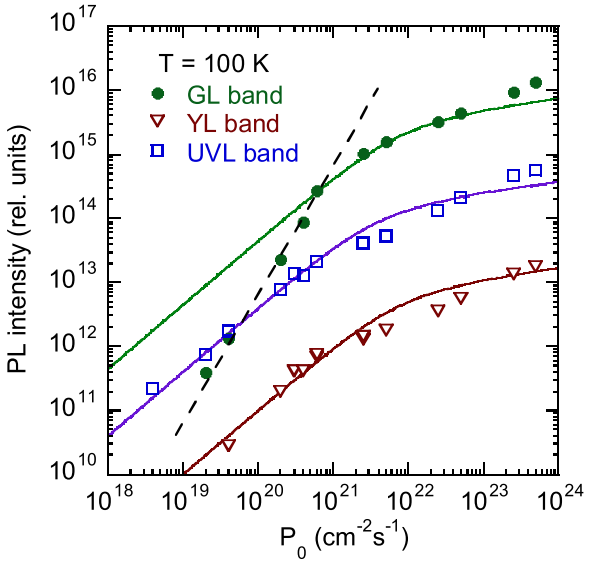

FIG. 10. (Color online) The dependences of PL intensity after a laser pulse on excitation intensity for PL bands in sample RS280 at 100 K. The solid lines are calculated using Eq. (37) of Ref. [30], with the following parameters: $\eta_0 = 0.0018$; $\tau_0 = 4.5\,\mu$s; and $N = 5 \times 10^{14}\,\mathrm{cm^{-3}}$ for the GL band; $\eta_0 = 0.0018$; $\tau_0 = 2$ ms; and $N = 5 \times 10^{14}\,\mathrm{cm^{-3}}$ for the YL band; and $\eta_0 = 0.004$; $\tau_0 = 100\,\mu$s; and $N = 5 \times 10^{14}\,\mathrm{cm^{-3}}$ for the UVL band. The dashed line indicates the quadratic dependence of PL intensity on the excitation intensity.

To estimate the contribution of the C_N-related YL band to the PL spectra at different excitation intensities, we assumed that the hole-capture coefficients for the $-/0$ and $0/+$ levels of the C_N defect (for the YL and GL bands, respectively) are similar. The expected intensity of the YL band is shown with a dotted curve in Fig. 8. Note that if the hole capture coefficient for the $-/0$ level is higher, the intensity of the YL will shift upward by the same factor. While the YL band with such intensity could not be observed in the steady-state PL spectrum at any excitation intensity, it can be revealed in time-resolved PL measurements.

Figure 9 shows the evolution of the PL spectrum for the same sample after a pulsed excitation at $T = 100\,\mathrm{K}$. For short time delays (up to 10^{-5} s), the GL band is the dominant band in the defect-related part of the spectrum. For longer time delays, the GL band disappears, and the YL band with a maximum at 2.1 eV emerges (Fig. 9). The shape of the YL band in Fig. 9 is fit using Eq. (1) with the same parameters, $\hbar\Omega$ and S_e, as for the YL band in Fig. 2. However, $\hbar\omega_{\max} = 2.1\,\mathrm{eV}$ and $E_0 = 2.57\,\mathrm{eV}$ had to be taken for the best fit in Fig. 9 instead of 2.2 and 2.64 eV, respectively, which were used in Fig. 2. An example with the latter parameters is shown in Fig. 9 as the dashed curve 4′. This indicates that these two YL bands originate from two different sources. At longer delay times (longer than 10^{-3} s), the YL band gradually disappears as it is obscured by the RL band. The BL, GL, YL, and RL bands can be reliably observed in time-resolved PL spectra because they have different PL lifetimes at 100 K: 500 μs (BL band), 4.5 μs (GL band), 2 ms (YL band), and ∼6 ms (RL band).

The dependences of the peak intensity on the excitation intensity for the GL, YL, and UVL bands at 100 K are shown in Fig. 10. The intensities of the UVL and YL bands increase linearly with increasing excitation intensity up to $\sim 10^{22}\,\mathrm{cm^{-2}s^{-1}}$ and saturate at higher excitation intensities. However, the intensity of the GL band increases as a square of the excitation intensity for $P_0 < 10^{21}\,\mathrm{cm^{-2}\,s^{-1}}$ (dashed line in Fig. 10). These results are consistent with those obtained from steady-state PL, suggesting that two holes are captured by the defect when producing the GL band, while only one hole is captured by the same defect when producing the YL band.

2. *Less pure GaN (strong YL and weak GL)*

Figures 11 and 12 show evolutions of the PL spectra with excitation intensity (for steady-state PL) and with time (after a laser pulse) for sample 1007. In steady-state PL spectra, the GL band appears to contribute only at high excitation intensity as a weak shoulder to the stronger YL band. The RL, YL, and GL bands significantly overlap and are difficult to resolve. To deconvolute the bands, we simulated the shapes of the YL and GL bands by using Eq. (1), with the parameters given in the captions of Figs. 2 and 4, respectively, while the shape of the RL band was taken from other samples in which the RL band was the dominant defect-related PL band [28]. The intensities of the RL band in samples RS280 and 1007 were almost the same, whereas the YL band was at least an order of magnitude stronger in sample 1007 as compared to sample RS280 (where it could not be seen in the steady-state PL spectra).

In the PL spectrum obtained after a pulsed excitation, the GL band and the YL band can be clearly seen at short and long time delays, respectively (Fig. 12). In contrast to sample RS280 (with $\hbar\omega_{\max} = 2.1\,\mathrm{eV}$ for the YL band), the YL band has a maximum at 2.2 eV and the same shape as for GaN

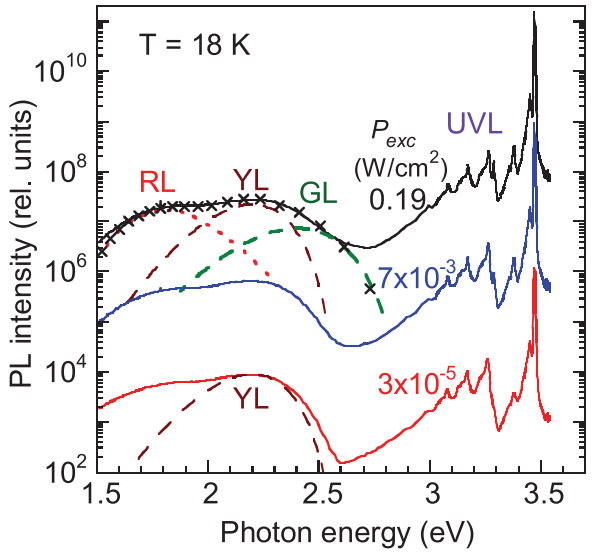

FIG. 11. (Color online) The steady-state PL spectra at $T = 18$ K and different excitation intensities for sample 1007. In the defect-related region of the spectra, the contributions from four PL bands can be found: UVL, GL, YL, and RL. The dashed and dotted curves show an example of deconvolution. The crosses show the sum of the GL, YL, and RL bands used for the deconvolution of the PL spectrum at $P_{\rm exc} = 0.19\,{\rm W/cm^2}$.

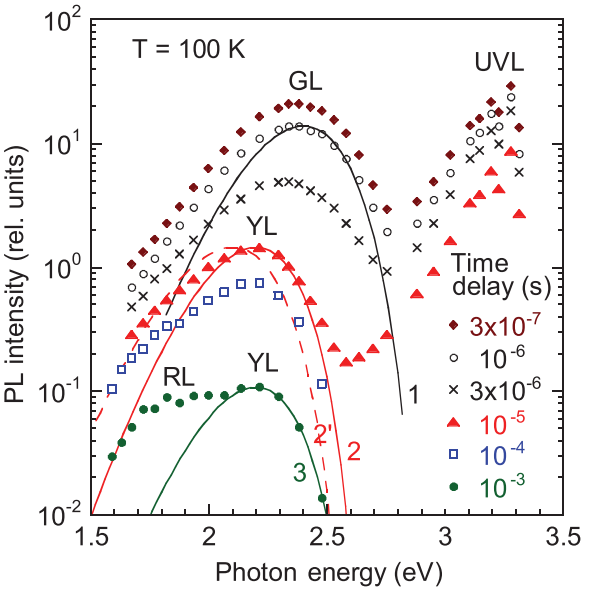

FIG. 12. (Color online) PL spectra at different time delays after a pulsed excitation with $P_0 = 5 \times 10^{21}\,{\rm cm^{-2}s^{-1}}$ for sample 1007. The symbols are experimental points, and the curves are calculated using Eq. (1), with the following parameters: $S_e = 8.5$; $E_0 = 2.9$ eV; $\hbar\omega_{\rm max} = 2.4$ eV; and $\hbar\Omega = 41$ meV (curve 1); $S_e = 7.4$; $E_0 = 2.64$ eV; $\hbar\omega_{\rm max} = 2.2$ eV; and $\hbar\Omega = 56$ meV (curves 2 and 3). The dashed curve 2′ corresponds to the YL band shown in Fig. 9, with $S_e = 7.4$; $E_0 = 2.57$ eV; $\hbar\omega_{\rm max} = 2.1$ eV; and $\hbar\Omega = 56$ meV.

samples grown by MOCVD. An example with the parameters of the YL band with $\hbar\omega_{\rm max} = 2.1$ eV is shown in Fig. 12 as the dashed curve 2′. The different positions of the YL band maxima in time-resolved PL measurements for samples RS280 and 1007 are the first indication of the fact that the YL bands in these two samples are caused by two different defects. An additional piece of evidence for this follows from the analysis of the decays of the YL and GL bands after a laser pulse, which is discussed below.

3. *Decay of the GL and YL intensity after a laser pulse*

Figure 13 shows the decay of PL intensity at 2.3 eV and 100 K after a laser pulse for three HVPE-grown samples. Since the PL intensity integrated over photon energies is nearly the same for the YL and GL bands when they are normalized at their maxima, and the PL intensities at 2.3 eV for the normalized bands are equal (∼85% from their peak intensities), the PL intensity at 2.3 eV is proportional to the number of photons emitted at any time via *both* the YL and GL mechanisms. Moreover, the relative number of photons emitted *separately* via the YL and GL mechanisms can be found by integrating this intensity over time in the range of short time delays (where the GL band dominates and the contribution of the YL band is negligible) and at longer time delays (where the GL band vanishes and only the YL band remains). The dependence of PL intensity on time, $I^{\rm PL}(t)$, can be fit with the following equation:

$$I^{\rm PL}(t) = I^{\rm PL}(0)\exp(-t/\tau)\,. \qquad (5)$$

The exponential decay for times shorter than 10^{-5}–10^{-4} s corresponds to the decay of the GL band with lifetime τ ranging from 1.8 to 4.5 μs for different samples. For longer time delays, the nearly exponential decay corresponds to the decay of the YL band with τ ranging from 0.3 to 1.85 ms. The PL intensities were integrated over time, separately for the short-living GL and for the long-living YL (inset in Fig. 13). The ratio of the GL band intensity to the YL band intensity in these measurements is 2.4 for sample B73, 1.7 for sample RS280, and 0.18 for sample 1007. Note that these measurements were conducted at high excitation intensity, corresponding to the saturation regime (Fig. 10). If the GL and YL bands in these samples were related to the $-/0$ and $0/+$ states of the same defect and if after each pulse, equilibrium in the dark was completely achieved, then the *integrated over time* intensities of the GL and YL bands in time-resolved measurements should be equal. Indeed, when all the C_N defects are saturated with two holes, the same number of photons should be emitted from these defects when they lose the first hole in the process of fast electron-hole recombination (the GL band) and when they subsequently lose the second hole at longer time delay (the YL band).

The small prevalence of the time-integrated GL intensity over the YL intensity in samples B73 and RS280 can be explained by incomplete restoration of the dark equilibrium. Such an assumption is supported by the observation of a slower-than-exponential tail of the YL band (Fig. 13). This may be due to small contributions from donor-acceptor pair (or shallow donor-deep donor pair) transitions at 100 K, which persist for a long time [32]. Since the restoration appears to be incomplete (the next pulse arrives before all the defects become completely filled with electrons), the integrated over

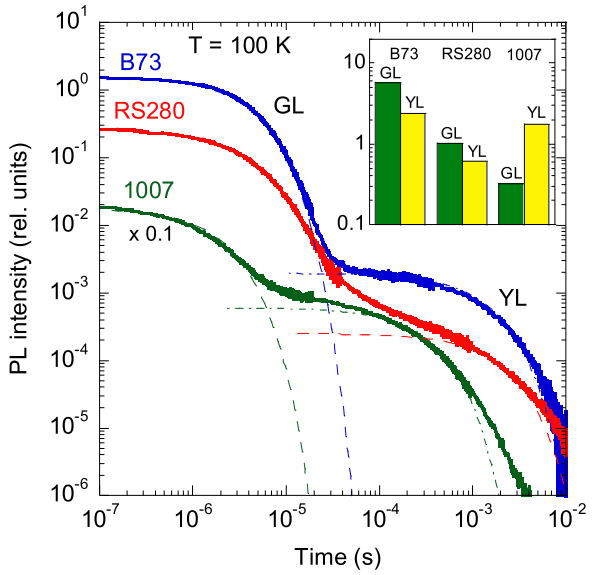

FIG. 13. (Color online) Decay of PL after a laser pulse for three HVPE GaN samples at 100 K. The emission photon energy is 2.3 eV, at which the intensities of the GL and YL bands are close to the intensities in their maxima. The intensity for sample 1007 is multiplied by 0.1 for clarity. The dashed and dash-dotted curves are calculated using Eq. (5), with the following parameters: $I^{\mathrm{PL}}(0) = 1.6$ and $\tau = 3.6\,\mu$s (GL band) and $I^{\mathrm{PL}}(0) = 1.95 \times 10^{-3}$ and $\tau = 1.3$ ms (YL band) for sample B73; $I^{\mathrm{PL}}(0) = 0.23$ and $\tau = 4.5\,\mu$s (GL band) and $I^{\mathrm{PL}}(0) = 2.5 \times 10^{-4}$ and $\tau = 1.85$ ms (YL band) for sample RS280; and $I^{\mathrm{PL}}(0) = 0.018$ and $\tau = 1.8\,\mu$s (GL band) and $I^{\mathrm{PL}}(0) = 6 \times 10^{-4}$ and $\tau = 0.3$ ms (YL band) for sample 1007. The inset shows the integrated over time intensities of the GL and YL band components in relative units.

time intensity of the YL band related to the $-/0$ level of C_N is expected to be lower than that of the GL band. This agrees with the data for samples B73 and RS280 in the inset to Fig. 13. However, the prevalence of the YL intensity over the GL intensity by almost an order of magnitude in sample 1007 indicates that a stronger YL band in this sample is *not* related to the C_N defect. We suggest that this stronger YL band is actually related to the C_NO_N complex.

D. Theoretical results

1. Formation energies and the choice of chemical potentials

Hybrid functional calculations, which have become widespread in semiconductor defect physics, are capable of accurately reproducing some of the defect properties, such as optical and thermodynamic transition levels [33]. On the other hand, the computed formation energies are difficult to directly compare with experiment, which is in part due to the difficulties in determining the elemental chemical potentials. In previous studies of defects in semiconductors, chemical potentials were often extracted from the bulk or molecule calculations of the most stable phases of chemical elements. Computed total energies of diamond [9] or graphite [34] were used for carbon chemical potentials and energies of oxygen and nitrogen in O_2 and N_2 molecules for O and N chemical potentials [7]. In principle, the chemical potentials for elements involved in the sample growth should be obtained from the formation enthalpies of the phases competing with the growth of GaN. Therefore, the chemical potential of oxygen, obtained from Ga_2O_3 rather than the O_2 molecule, is expected to better represent the formation energy of the oxygen defect in GaN (such as O_N). In addition, the competing phase needs to be identified for the chemical potential of nitrogen, since formation of this defect (O_N) depends on the energy balance of exchanging oxygen and nitrogen in the GaN lattice. For nitrogen, the formation of ammonia might represent a competing phase to the formation of GaN, if the growth involves significant amounts of hydrogen. To be consistent, one would need to apply the same procedure for all elemental chemical potentials; i.e., identify the competing phases for all elements involved in material formation and pick the lowest energy phases as those limiting the sample growth. However, given the variety of regimes and methods of growth, it is difficult to reliably predict all possible competing phases for all elements in the sample. In the above example of O_N, a growth regime which does not involve hydrogen would result in a different growth-limiting phase determining the chemical potential of nitrogen. Coupled with the nonequilibrium nature of crystal growth, this results in a wide variety of defect properties for different samples. Thus, it is difficult to expect that a single value of the chemical potential can lead to the computed defect formation energies that accurately represent actual defect concentrations in various samples. Therefore, only average general trends in defect formation could be captured if some averaged values of the chemical potentials can be determined.

Recently, Lany [35] suggested that the appropriate choice of chemical potentials (along with corrections to the host semiconductor band edges) results in accurate computed formation enthalpies of solid compounds [36,37]. These atomic chemical potentials, or fitted elemental-phase reference energies (FERE) [37], are obtained by fitting their values into a large set of measured formation enthalpies. As a result, FERE chemical potentials provide a better error cancellation for predicting formation enthalpy values of binary, ternary, and quaternary compounds, when chemical bonding is formed between metals and nonmetals, and the energy differences have to be computed between chemically different systems. Thus, compared to the chemical potentials obtained from calculations of elemental bulk phases or molecules, the FERE energies can provide more reliable average formation energies of defects.

In this paper, for the chemical potentials of oxygen and nitrogen, we used FERE energies obtained from the HSE hybrid functional [36]. The resulting negative formation energy of O_N (see below), is in accord with a significantly larger absolute value of (negative) formation enthalpy of gallium oxide, compared to that of gallium nitride. For comparison we also calculated formation energies of oxygen related defects using the chemical potential of oxygen obtained from the formation enthalpy of Ga_2O_3. The chemical potentials of carbon, silicon, and gallium have been obtained from HSE calculations of bulk diamond, silicon, and metal orthorhombic gallium. We need to stress that optical and thermodynamic transition levels are unaffected by the choice of chemical

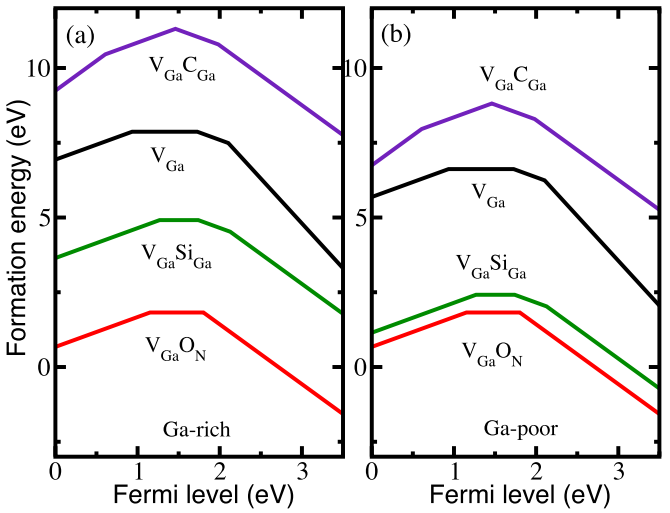

FIG. 14. (Color online) (a) Formation energies of the V_{Ga} and its complexes as a function of the Fermi energy for Ga-rich (a) and Ga-poor (b) growth conditions. For $V_{Ga}O_N$, the $2-/0$ charge state line intersection is at ∼1.8 eV above the VBM, with the $-/0$ and $2-/-$ transition levels being very close to each other: 1.85 and 1.76 eV, respectively.

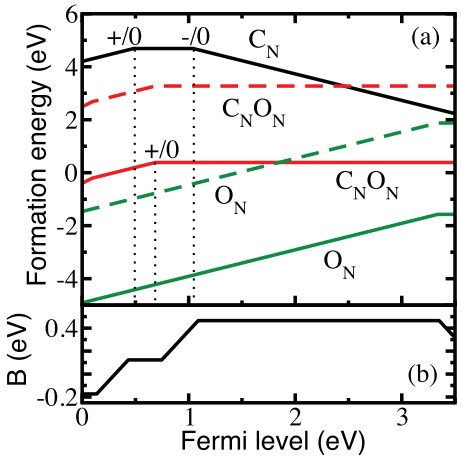

FIG. 15. (Color online) (a) Formation energies of carbon acceptor C_N, oxygen donor O_N, and donor-acceptor complex C_NO_N defects in GaN as a function of the Fermi energy. Solid and dashed lines for O_N and C_NO_N correspond to two different oxygen chemical potentials (see text). Dotted lines indicate transition levels responsible for the observed PL bands. (b) Binding energy of the C_NO_N complex.

potentials, since they are formation energy differences. Therefore, unlike the absolute values of the formation energies, the computed transition levels can be directly compared with the experiment.

2. Gallium vacancy complexes

First, we present the results of calculations for the V_{Ga}-related complexes. For more than a decade, a V_{Ga} or its complex with oxygen were considered to be the major candidate for the defect causing the YL band both by experimentalists and theorists [5]. Previous density functional theory (DFT)-based calculations predicted that the V_{Ga} is a deep acceptor with multiple charge states, from neutral to $3-$ [38,39]. Therefore, a logical assumption was that in n-type GaN, positively charged shallow donors, such as silicon or carbon substituting gallium (Si_{Ga}, C_{Ga}) and oxygen substituting nitrogen (O_N), could be bound to the $3-$ charged V_{Ga} to form complexes. Based on the PL measurements and extensive positron annihilation data, it was suggested that the $V_{Ga}O_N$ complex is responsible for the YL and GL bands in n-type GaN [5,6]. Here, we examine the case of the vacancy-containing complexes in GaN by using the hybrid functional calculations.

Figure 14 shows the formation energies as a function of the Fermi energy in the band gap for the isolated V_{Ga} and three V_{Ga} complexes in both Ga-rich and Ga-poor growth conditions. The slopes of the formation energy lines represent the charge states of a defect, and the points of intersection indicate the thermodynamic transition levels. The $V_{Ga}C_{Ga}$ complex exhibits high formation energies in both Ga-rich and Ga-poor environments and therefore is unlikely to form. Furthermore, the computed binding energy for this complex is negative, implying that the interaction between V_{Ga}^{3-} and C_{Ga}^{+} is repulsive. Both $V_{Ga}Si_{Ga}$ and $V_{Ga}O_N$ complexes are stable and have relatively low formation energies, especially in a Ga-poor growth environment. However, as shown in Fig. 14, the $-/0$ and $2-/-$ thermodynamic transition levels for these complexes are too high above the VBM to be responsible for either the YL band or the GL band. In particular, the $V_{Ga}O_N$ complex forms a negative-U center, where the $-/0$ transition level is higher than $2-/-$ level, 1.85 and 1.76 eV above the VBM, respectively. The related PL bands in n-type GaN are expected to have a maximum at 1.53 eV (for transitions via the $2-/-$ level) and 1.24 eV (via the $-/0$ level). Thus, $V_{Ga}O_N$ complex would produce PL bands in the infrared region. Similar results are obtained for the $V_{Ga}Si_{Ga}$ complex, where the $-/0$ and $2-/-$ thermodynamic transition levels are computed to be at 1.74 and 2.13 eV above the VBM (Fig. 14). This leads to optical transitions of 1.13 and 0.7 eV for transitions via the $-/0$ and $2-/-$ transition levels, respectively, which are also in the infrared region. Finally, as shown in Fig. 14, the isolated V_{Ga} also has a deep $3-/2-$ transition level (2.06 eV above the VBM), and the PL band maximum (if the V_{Ga} is present and behaves as a radiative defect) would be also in infrared. Similar value for the $3-/2-$ transition level was recently obtained by Gillen and Robertson by using the screened-exchange local density approximation (LDA) method [40]. Thus, neither isolated V_{Ga} nor the V_{Ga}-containing complexes can account for the YL or GL bands in GaN.

3. Formation of carbon- and oxygen-related defects

Figure 15(a) shows the formation energies of carbon- and oxygen-related defects as a function of the Fermi energy in the band gap. Overall, in n-type GaN, the formation energies of oxygen donors are significantly lower (by ∼3.8 eV) than those of carbon acceptors, while the formation energy of the C_NO_N complex is ∼1.8 eV lower than that of C_N. These results are obtained using the elemental chemical potentials described in Sec. III D 1. In Fig. 15, the chemical potential of nitrogen

is not adjusted by the formation enthalpy of GaN, and the results represent the nitrogen-rich conditions, as commonly referred to in the literature. While oxygen is the most abundant donor in GaN in most cases, the concentration of carbon can exceed that of oxygen in some MOCVD samples (Table I). However, even with the same growth method (MOCVD), both conductive samples (with more oxygen donors) and insulating samples (with more carbon) can be obtained. This suggests that the absolute values of formation energy computed with any theoretical method, which assumes equilibrium conditions, are at best rough guidelines for expected relative concentrations of impurities. The SIMS measurements suggest that the nonequilibrium incorporation of carbon into GaN (in either the C_N acceptor or C_NO_N configuration) in some cases could be similar to that of the oxygen donor O_N. For comparison, dashed lines in Fig. 15(a) show the results for O_N and C_NO_N computed using the oxygen chemical potential obtained from Ga_2O_3. In this case, the formation energies of C_N and O_N become comparable (which could be the case in some MOCVD samples). Thus, different competing phases during different regimes of growth can create favorable conditions for the formation of either isolated carbon acceptor C_N, in some cases, or the C_NO_N complex, in other cases.

The thermodynamic transition levels of the C_N acceptor, C_NO_N complex, and O_N donor have been published elsewhere [7,9]. The C_N acceptor is found to have two transition levels [Fig. 15(a)]: the $0/+$ transition level at 0.48 eV above the VBM and the $-/0$ transition level at 1.04 above the VBM. Interestingly, a defect commonly thought of as an acceptor can also exhibit a donor-like $+$ charge state. This is due to several electronic states that the defect creates in the band gap. For example, both C_N and C_NO_N create three electronic defect states in the band gap (shown in Ref. [7]). In the neutral state of C_N, two of these defect states are occupied by electrons (all three states are occupied in $C_NO_N^0$). The addition of an electron leads to the $-/0$ transition level, and the removal of an electron leads to the $0/+$ level in the band gap. Detailed calculations show that numerous defects have multiple charge states in wide band gap semiconductors, especially defect complexes that often create multiple defect states in the band gap.

The $0/+$ transition level of the O_N donor is found to be 0.14 eV below the CBM. The transition levels for the C_NO_N complex are 0.14 eV above the VBM for the $+/2+$ level and 0.75 eV for the $0/+$ level. The $-/0$ transition level of C_N is deeper than the $0/+$ level of C_NO_N complex, suggesting that the YL band generated by C_N should be shifted to energies lower than that from the C_NO_N complex.

Most importantly, the calculations presented in Fig. 15 confirm that the difference in the transition level structure for the two carbon defects (C_N and C_NO_N) allows for the possibility to distinguish between the different sources of the YL band. In samples where carbon is mostly bound into the C_NO_N complex, only a single YL band should be observed since there is only one possible transition, via the $0/+$ level. However, if carbon exists mostly in the form of isolated C_N defects, two PL bands are possible. Along with the YL band caused by transitions via the $-/0$ level of C_N, the secondary PL band can be activated by increasing optical excitation intensity. This will happen when a second hole is captured by a neutral C_N defect, with subsequent emission via the $0/+$ level of the C_N defect.

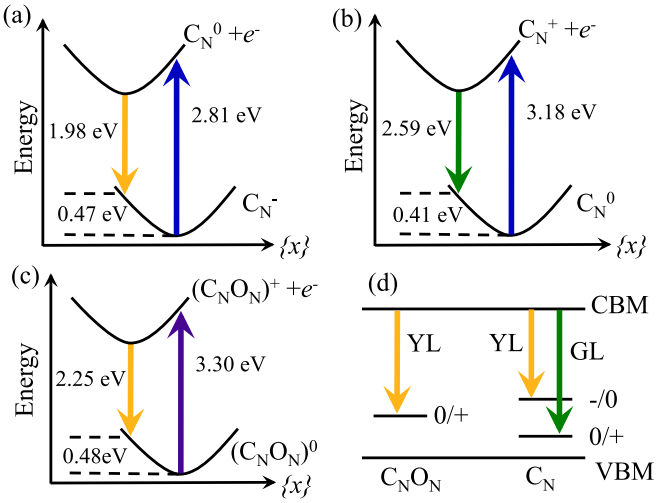

FIG. 16. (Color online) Schematic configuration coordinate diagrams for the C_N acceptor (a) and (b) and for the C_NO_N donor (c). The optical transitions are shown with arrows: downward for PL (emission) and upward for the resonant excitation of a defect (absorption). (a) Absorption and emission via the $(-/0$ transition level of C_N; (b) transitions via the $0/+$ level of C_N; (c) transitions via the $0/+$ level of the C_NO_N complex; and (d) band diagram with transition levels.

4. *Optical transitions*

Due to the existence of the three carbon-related transition levels, the $0/+$ and $-/0$ levels for C_N and the $0/+$ level for C_NO_N, three well-separated PL bands can be observed experimentally in the visible part of the spectrum. Figure 16 illustrates the optical transitions via the C_N and C_NO_N defects.

While optical transitions via the isolated carbon acceptor C_N have been suggested to produce the YL band [8], we find that the transitions via this acceptor should produce a PL band with a maximum at 1.98 eV and a ZPL at 2.45 eV. In n-type GaN, this acceptor is negatively charged in the ground state (Fig. 15). Once the electron-hole pair is created with above-band-gap laser illumination, the hole is captured by the negatively charged acceptor in $\sim 10^{-10}$ s, changing its charge state to neutral (if the defect were excited resonantly with below-band-gap light, the maximum of the characteristic excitation band would be at 2.81 eV, according to our calculations). Since the PL lifetime is relatively long, a second hole can be captured by the neutral C_N defect due to the existence of the $0/+$ transition level of C_N in the band gap. As a result, radiative recombination can occur, with a free electron recombining with a hole at C_N^+. This transition is shown with a downward arrow in Fig. 16(b). The energy of this transition is computed to be 2.59 eV and is between green and blue in the visible range. The ZPL for this transition is computed to be 3.00 eV. The yellow (or orange) PL band with a maximum at 1.98 eV is generated by the C_N defect and should have a lower PL band maximum than the PL band generated by the C_NO_N complex [Fig. 16(c)]. The C_NO_N complex is expected

to produce a PL band with a maximum at 2.25 eV and a ZPL at 2.73 eV.

Overall, the calculated trends are such that in samples where carbon is bound into the C_NO_N complex, only one PL band (yellow) is possible, while in samples where the carbon is predominantly isolated as the C_N acceptor, two PL bands are possible: yellow (or orange) and green (or green-blue). These trends are in quantitative agreement with experimental data, as will be discussed in Sec. IV.

Finally, it may appear surprising that both donors and acceptors can cause the YL band in GaN. It is commonly thought that an acceptor is a much more natural candidate for this process, since a negatively charged acceptor should capture holes more efficiently. However, a neutral deep donor is also capable of capturing a hole, albeit with a capture cross section lower by about an order of magnitude [41]. In addition, some published results of electron paramagnetic resonance measurements indicate that the YL band is associated with a deep donor rather than an acceptor [42]. The g factors determined for the YL band with a maximum at 2.2 eV ($g_{||} = 1.989$ and $g_{\perp} = 1.992$) are smaller than the free electron value of g, which indicates that the related defect may indeed be a deep donor [42].

5. *Stability of the C_NO_N complex*

The binding energy B of the C_NO_N complex for a range of Fermi energies is shown in Fig. 15(b). While this complex is unstable in p-type GaN, the binding energy of this complex in n-type GaN is 0.46 eV. Since the complex is formed by the next nearest neighbor atoms in the GaN lattice, this binding energy is relatively low. However, the binding energy provides limited information about the stability of the complex. In order to estimate the stability of the complex, we calculated the C_NO_N complex dissociation barriers using HSE and generalized gradient approximation (GGA).

The C_NO_N complex can dissociate by the jump of either a C or O atom into an interstitial site, leaving behind a nitrogen vacancy (V_N). However, our HSE calculations for n-type GaN show that the formation energies are high for stable interstitial O_i and split-interstitial C_i: 3 to 5.5 eV higher than those of the O_N and C_N defects, which agrees with previously published results [9,43,44]. Additionally, our calculations show that in the presence of the V_N formed in place of the C_N or O_N defects, both the split-interstitial carbon and interstitial oxygen are unstable. Therefore, the dissociation of the C_NO_N complex via diffusion of either oxygen or carbon into the nearest interstitial sites is energetically unfavorable.

Even if a V_N was already present as a nearest neighbor of the C_NO_N complex (which is unlikely, due to the negligible concentrations of V_N in n-type GaN and the absence of attractive interaction between V_N and C_NO_N), migration of oxygen into the V_N would not be favorable. The nudged elastic band calculations based on GGA reveal a diffusion barrier for this process of 1.7 eV. Assuming the typical phonon frequency of 10^{13} s^{-1} and following Ref. [45], we estimate that in this case, the complex remains stable for temperatures up to ~660 K. Thus, when the C_NO_N complexes are formed during growth, they are likely stable.

IV. DISCUSSION

A. Yellow and blue luminescence bands in undoped and C-doped GaN

In MOCVD-grown n-type GaN, only the YL band is observed in the defect-related part of the PL spectrum (Fig. 2). With increasing excitation intensity, the YL band intensity saturates, and no other bands appear at higher photon energies. If the YL band in this sample was caused by electron transitions via the $-/0$ state of the isolated C_N defect, then it is expected that a PL band related to transitions via the $0/+$ level should emerge at higher photon energies, which is not observed in Fig. 2. Thus, the absence of any PL band in the range from 2.6 to 3 eV in n-type GaN (Fig. 2) is an indication that the YL band in the MOCVD-grown GaN (sample EM1256) is not related to the isolated C_N defect. In contrast, the C_NO_N complex can explain the YL in this sample, since it does not have the transition levels necessary to produce an additional PL band in this range.

In the literature, there is controversial information regarding the blue band in GaN, which, according to Ref. [9], could be assigned to the $0/+$ transition level of the C_N acceptor. A careful analysis suggests that this is unlikely. Indeed, a blue band is often observed in C-doped GaN, along with the YL band [10–13,46]. However, closer inspection of the luminescence spectra in these papers allows us to conclude that at least two different defect-related blue bands were observed. A band with a maximum at 2.85–2.86 eV (the BL band) was observed in GaN grown by molecular beam epitaxy (MBE) [12,13], and a broader band with a maximum at 3.0 eV (the BL2 band) was observed in GaN grown by MOCVD [10,11]. In Ref. [12], where the excitation intensity was extremely high (400 kW/cm^2), the intensity of the YL band was about an order of magnitude higher than that of the BL band in all of the high-resistivity GaN samples doped with carbon. This is inconsistent with a model according to which the YL and BL bands are caused by two charge states of the same defect [9]. Indeed, the intensity of the YL band should be much lower than that the BL band since the defect is almost completely saturated with holes in such experimental conditions. At lower excitation intensities (20 W/cm^2), the intensity of the BL band (relative to the YL band) decreased with increasing concentration of C from 2×10^{18} to 2×10^{19} cm^{-3} [13]. We assume that the BL band observed in Refs. [12,13] is caused by the Zn_{Ga} acceptor, since the BL band with a maximum at 2.9 eV is strong even at low levels of contamination with Zn (lower than 10^{16} cm^{-3}) [5]. It is also unlikely that the BL band in C-doped GaN is related to Mg, because the Mg-related BL band appears only in GaN heavily doped with Mg, and it greatly shifts with increasing excitation intensity [47]. No shifts were observed for the BL band in the MBE-grown GaN. [13].

In MOCVD-grown GaN, a broad band with a maximum at 3.0 eV is identified as the BL2 band [24,25]. The BL2 band is quenched above 75 K with an activation energy of about 150 meV [25], which is very similar to the results reported in Ref. [11]. It is interesting to note that a very similar quenching of the BL2 band with increasing temperature from 15 to 150 K and the dominance of the Zn-related BL band at higher temperatures was observed in Refs. [13,25]. The BL2 band demonstrates a characteristic metastable behavior; namely,

it bleaches considerably under continuous above-band-gap illumination, as the YL band simultaneously rises [25]. The bleaching has been attributed to a recombination-assisted dissociation of a defect complex, apparently containing hydrogen as a component [5]. A very similar behavior of the 3.0 eV band in C-doped GaN was reported in Ref. [11]. Note that a strong blue band with a maximum at 3.05 eV was observed in C-doped ($[C] = 1.5 \times 10^{18}\,cm^{-3}$), conductive ($n = 10^{18}\,cm^{-3}$) GaN grown by MOCVD [46]. The blue band in Ref. [46] became much stronger than the YL band after treatment in hydrogen plasma at 200 °C for 1 h. This may indicate that the authors of Ref. [46] observed the BL2 band related to a defect complex containing hydrogen. In some GaN samples (undoped, C doped, and Fe doped), the fine structure of the BL2 band is observed, with the ZPL at 3.34 eV [25]. From the position of the ZPL, it was suggested that the transition level responsible for the BL2 band is located at 0.15 eV above the valence band [24]. Summarizing the above information, we suggest that blue bands sometimes observed in C-doped GaN have no relation to the isolated C_N defect.

B. Yellow and green luminescence bands in GaN grown by HVPE

The GL band with a maximum at 2.4 eV is observed only in high-quality GaN grown by the HVPE technique. In freestanding GaN (sample B73), the defect responsible for the GL band is the dominant deep-level defect, with a concentration of about $10^{15}\,cm^{-3}$ (Ref. [6]). From temperature-dependent Hall effect measurements, the total concentration of acceptors in a similar sample has been estimated to be $2.4 \times 10^{15}\,cm^{-3}$ (Ref. [48]). From the SIMS analysis of similar freestanding GaN, it was found that the concentrations of oxygen and carbon are on the order of $10^{16}\,cm^{-3}$ each, where the O_N defect (with a concentration of $7.8 \times 10^{15}\,cm^{-3}$ from Hall effect measurements) is the main shallow donor in these samples [49,50]. Since the GL band intensity increases as a square of the excitation intensity [6], it is reasonable to attribute this band to transitions of electrons from the conduction band to the $0/+$ level of the C_N defect. In this case, the YL band can be caused by transitions via the $-/0$ level of the same defect.

Analysis of the time-resolved PL spectra in GaN samples exhibiting a strong GL band (Fig. 9 for sample RS280 and Fig. 4 in Ref. [51] for freestanding GaN) indicates that the YL band, related to the $-/0$ level of C_N, has a maximum at 2.1 eV. In these high-purity HVPE samples, the integrated over time intensity of the YL band after pulsed excitation is only slightly lower than that of the GL band (inset in Fig. 13), which is in agreement with the assumption that the YL band and the GL band are associated with transitions via different charge levels of the same defect.

However, in less pure HVPE samples (such as sample 1007) and apparently all MOCVD samples, another defect is responsible for the dominant YL band, which has a maximum at 2.2 eV. Previously, we attributed this YL band to the C_NO_N complex [7]. The saturation of this YL band in MOCVD samples is not followed by the emergence of any other PL band at higher photon energies (Fig. 2). This suggests that in MOCVD samples the YL band is produced by the C_NO_N complex, and isolated carbon C_N is not found.

On the other hand, in HVPE-grown GaN layers on sapphire (more than 20 samples studied in this paper), the intensities of the YL bands originating from the C_N and C_NO_N defects may be comparable. For the samples of highest purity, such as sample RS280, the C_N-related band is the dominant YL band. In these samples, the integrated over time intensities of the YL and GL bands after a laser pulse are nearly equal to each other, which is consistent with the assignment of these bands to two different charge states of the same defect. In less pure samples, such as sample 1007, the C_NO_N-related YL band is dominant. In this case, the integrated over time intensity of the YL band is about 10 times higher than that for the GL band. Thus, we expect that in this sample, the concentration of the C_NO_N defects is higher than that of the C_N defects by roughly an order of magnitude. It appears that only in GaN samples with very low concentrations of carbon and oxygen impurities, the isolated C_N defects may be the dominant defects causing the YL and GL bands, whereas in samples with relatively high concentration of either C, O, or both, the C_NO_N complexes are likely to be formed and will cause the YL band but not the GL band.

C. Comparison of theory and experiment

The experimental and theoretical findings are summarized in Table III. The characteristic excitation band maximum, $\hbar\omega_{max}^{exc}$, for the YL band (assumed to be related to the C_NO_N complex) in GaN was estimated to be 3.19 eV (Ref. [52]) and 3.32 eV (Ref. [53]) from the analysis of the shape of the PL excitation (PLE) spectrum. Note that a significant part of the characteristic excitation band was obscured in these experiments due to the contribution of band-to-band excitation in the PLE spectrum. We expect that this may result in an uncertainty of about ± 0.1 eV in the determination of $\hbar\omega_{max}^{exc}$. The experimental value of the ZPL for the YL band (2.64–2.70 eV) was found as the middle point between the threshold of the PL band and that of the PLE band [5,52]. The experimental values of ZPL for the C_N-related GL and YL bands in the studied HVPE-grown GaN samples were estimated from the best fits of the PL band shape with Eq. (1). To account for possible errors in these estimates, we rounded the values and added tilde marks in Table III. The distance of the defect level from the VBM, E_A, was calculated as the difference between the band-gap energy and the ZPL.

Overall, the experimental values agree very well with the calculated ones. In most cases, the disagreement between calculations and experiment does not exceed 0.1 eV. The close agreement allows us to draw the conclusion that there are two separate sources of the YL band in different samples, namely, the isolated C_N defect and the C_NO_N complex. These two cases can be distinguished by the presence of the GL band only in some high-quality samples containing mostly isolated C_N acceptors.

D. V_{Ga}-related defects as a source of the YL band

According to our hybrid functional calculations, neither V_{Ga} nor its complexes with O_N, Si_{Ga}, or C_{Ga} can be responsible

TABLE III. Comparison of theory and experiment for observed PL bands and suggested defect configurations. Experimental values are taken from this work and from Refs. [5,52].

PL band (defect)	Level		$\hbar\omega_{max}$ (eV)	$\hbar\omega_{max}^{exc}$ (eV)	ZPL (eV)	E_A (eV)
GL (C_N)	0/+	Experiment	2.4	–	∼2.9	∼0.6
		Theory	2.59	3.18	3.00	0.48
YL (C_N)	−/0	Experiment	2.1	–	∼2.5–2.6	∼0.9–1.0
		Theory	1.98	2.81	2.45	1.04
YL (C_NO_N)	0/+	Experiment	2.2	3.19–3.32	2.64–2.70	0.8–0.86
		Theory	2.25	3.30	2.73	0.75

for the YL band, since optical transitions for these defects are expected in the infrared part of the spectrum. The correlations reported in the literature between the YL band intensity and the concentration of the V_{Ga}-containing defects could be accidental and the result of changes in other defect concentrations such as carbon. For example, in Ref. [54], the YL intensity increased almost linearly with the concentration of Ga vacancies for a few data points. However, the YL band in this paper was measured from the GaN/sapphire interface, where the concentration of various defects (other than V_{Ga}) is very high and may not be the same across the different samples. In another paper [17], the anticorrelation between the YL intensity and the concentration of the V_{Ga}-containing defects was observed for three high-resistivity GaN samples. Xu *et al.* [55] noticed that in GaN samples with undetectable amount of Ga vacancies, the YL intensity was significantly *higher* than that in GaN samples containing V_{Ga} with the concentration of $\sim 10^{17}$ cm^{-3}. Suihkonen *et al.* [56] also noted that the YL band in GaN is not related to Ga vacancies because no increase of the YL intensity with increasing concentration of V_{Ga} was observed. In spite of the contradictory data regarding the correlation between the YL intensity and the concentration of the V_{Ga}-containing defects, the idea that the YL band is caused by the $V_{Ga}O_N$ complex, at least in some GaN samples, is still widespread [57,58]. This attribution is based on the results of early DFT calculations [38,39]. However, our hybrid functional calculations show that the $V_{Ga}O_N$ complex (as well as the isolated V_{Ga} and its complexes with Si_{Ga} or C_{Ga}) have very deep transition levels in *n*-type GaN. The expected PL bands from the V_{Ga}-containing defects would be observed in the infrared part of the PL spectrum if these defects are radiative. Therefore, it is unlikely that V_{Ga}-related defects are responsible for the observed YL and GL bands.

V. CONCLUSIONS

The GL band with a maximum at 2.4 eV is observed only in high-purity GaN samples grown by the HVPE technique. This PL band is attributed to transitions of electrons from the conduction band to the 0/+ level of the C_N defect. According to first-principles calculations, the C_N defect has two transition levels: the −/0 level at 1.04 eV and the 0/+ level at 0.48 eV above the VBM. In *n*-type GaN grown by HVPE, the YL band with a maximum at 2.1 eV is caused by a recombination of free electrons with holes at the −/0 level of C_N at low excitation intensities, and it is replaced with the GL band at high excitation intensity. The intensity of the GL band increases as a square of the excitation intensity, in agreement with the assumption that two holes must be captured by the C_N defect before the GL band can be observed. The ZPL of the GL band is determined to be at 2.9 eV by simulating the shape of the GL band using a one-dimensional configuration coordinate model. This value agrees with the activation energy of 0.54 eV for the thermal emission of holes from the 0/+ level of C_N to the valence band, which explains the thermal quenching of the GL band for the temperature range 300–400 K. The YL band with a maximum at 2.1 eV is caused by transitions via the −/0 level of C_N. It can be observed in time-resolved PL spectra from some HVPE-grown samples, at time delays after a laser pulse when the much faster GL band vanishes. In other samples, it is buried under a stronger YL band of different origin, which has a maximum at 2.2 eV. The 2.2-eV band is the dominant PL band in undoped GaN grown by MOCVD. In our opinion, this band is caused by transitions of electrons from the conduction band (or from shallow donors at low temperatures) to the C_NO_N complex. It appears that in the majority of GaN samples, carbon impurities form complexes with oxygen and produce the YL band at 2.2 eV. Only in HVPE-grown GaN with a low concentration of carbon and oxygen defects, can luminescence from isolated C_N defects be observed as the YL band at 2.1 eV, which at high excitation intensities transforms into the GL band with a maximum at 2.4 eV.

ACKNOWLEDGMENTS

The authors are grateful to H. Morkoç from Virginia Commonwealth University (VCU), D. C. Look from Wright State University, and S. Guo and D. Gotthold from EMCORE Corp. for providing HVPE sample B73 and the MOCVD samples used in this paper. We also acknowledge Evans Analytical Group for SIMS measurements. The work at VCU was supported by grants from the National Science Foundation (DMR-1410125) and the Thomas F. and Kate Miller Jeffress Memorial Trust.

[1] Y. Saitoh, K. Sumiyoshi, M. Okada, T. Horii, T. Miyazaki, H. Shiomi, M. Ueno, K. Katayama, M. Kiyama, and T. Nakamura, Appl. Phys. Express **3**, 081001 (2010).

[2] Y. Wang, H. Xu, S. Alur, Y. Sharma, F. Tong, P. Gartland, T. Issacs-Smith, C. Ahyi, J. Williams, M. Park, G. Wheeler, M. Johnson, A. A. Allerman, A. Hanser, T. Paskova, E. A. Preble, and K. R. Evans, Phys. Status Solidi C **8**, 2430 (2011).

[3] J. Everts, J. van den Keybus, M. Van Hove, D. Visalli, P. Srivastava, D. Marcon, Kai Cheng, M. Leys, S. Decoutere, J. Driesen, and G. Borghs, IEEE Electron Device Lett. **32**, 1370 (2011).

[4] M.-W. Ha, C. H. Roh, D. W. Hwang, H. G. Choi, H. J. Song, J. H. Lee, J. H. Park, O. Seok, J. Lim, M.-K. Han, and C.-K. Hahn, Jpn. J. Appl. Phys. **50**, 06GF17 (2011).

[5] M. A. Reshchikov and H. Morkoç, J. Appl. Phys. **97**, 061301 (2005).

[6] M. A. Reshchikov, H. Morkoç, S. S. Park, and K. Y. Lee, Appl. Phys. Lett. **81**, 4970 (2002).

[7] D. O. Demchenko, I. C. Diallo, and M. A. Reshchikov, Phys. Rev. Lett. **110**, 087404 (2013).

[8] J. L. Lyons, A. Janotti, and C. G. Van de Walle, Appl. Phys. Lett. **97**, 152108 (2010).

[9] J. L. Lyons, A. Janotti, and C. G. Van de Walle, Phys. Rev. B **89**, 035204 (2014)

[10] C. H. Seager, A. F. Wright, J. Yu, and W. Götz, J. Appl. Phys. **92**, 6553 (2002).

[11] C. H. Seager, D. R. Tallant, J. Yu, and W. Götz, J. Lumin. **106**, 115 (2004).

[12] D. S. Green, U. K. Mishra, and J. S. Speck, J. Appl. Phys. **95**, 8456 (2004).

[13] R. Armitage, Q. Yang, and E. R. Weber, J. Appl. Phys. **97**, 073524 (2005).

[14] M. A. Reshchikov, J. Appl. Phys. **115**, 103503 (2014).

[15] D. C. Look, C. E. Stutz, R. J. Molnar, K. Saarinen, and Z. Liliental-Weber, Solid State Commun. **117**, 571 (2001).

[16] M. A. Reshchikov, R. H. Patillo, and K. C. Travis, in *Proceedings of the Materials Research Society Symposium*, edited by M. Kuball, T. Mukai, T. H. Myers, and J. M. Redwing (Materials Research Society, Warrendale, PA, 2006), Vol. 892, p. FF23.12

[17] F. Reurings and F. Tuomisto, Proc. SPIE **6473**, 64730M (2007).

[18] M. A. Reshchikov, A. Kvasov, T. McMullen, M. F. Bishop, A. Usikov, V. Soukhoveev, and V. A. Dmitriev, Phys. Rev. B **84**, 075212 (2011).

[19] M. A. Reshchikov, M. A. Foussekis, J. D. McNamara, A. Behrends, A. Bakin, and A. Waag, J. Appl. Phys. **111**, 073106 (2012).

[20] J. Heyd, G. E. Scuseria, and M Ernzerhof, J. Chem. Phys. **118**, 8207 (2003).

[21] H. Morkoç, *Handbook of Nitride Semiconductors and Devices* (Wiley, New York, 2008), Vols. 1–3.

[22] S. Lany and A. Zunger, Phys. Rev. B **78**, 235104 (2008).

[23] M. A. Reshchikov, D. O. Demchenko, J. D. McNamara, S. Fernández-Garrido, and R. Calarco, Phys. Rev. B **90**, 035207 (2014).

[24] M. A. Reshchikov and H. Morkoç, Physica B **376-377**, 428 (2006).

[25] M. A. Reshchikov, Y. T. Moon, X. Gu, B. Nemeth, J. Nause, and H. Morkoç, Physica B **376-377**, 715 (2006).

[26] M. A. Reshchikov, S. S. Park, K. Y. Lee, and H. Morkoç, Physica B **340-342**, 448 (2003).

[27] C. C. Klick and J. H. Schulman, Solid State Phys. **5**, 97 (1957).

[28] M. A. Reshchikov, A. Usikov, H. Helava, and Yu. Makarov, Appl. Phys. Lett. **104**, 032103 (2014).

[29] M. A. Reshchikov, Appl. Phys. Lett. **88**, 202104 (2006).

[30] M. A. Reshchikov, *Internal Quantum Efficiency of Photoluminescence in Wide-Bandgap Semiconductors, Chapter in Photoluminescence: Applications, Types and Efficacy*, edited by M. A. Case and B. C. Stout (Nova Science Publishers, Inc., New York, 2012), pp. 53–120.

[31] J. F. Muth, J. H. Lee, I. K. Shmagin, R. M. Kolbas, H. C. Casey, B. P. Keller, U. K. Mishra, and S. P. DenBaars, Appl. Phys. Lett. **71**, 2572 (1997).

[32] M. A. Reshchikov, M. Zafar Iqbal, S. S. Park, K. Y. Lee, D. Tsvetkov, V. Dmitriev, and H. Morkoç, Physica B **340-342**, 444 (2003).

[33] D. O. Demchenko and M. A. Reshchikov, Phys. Rev. B **88**, 115204 (2013).

[34] A. F. Wright, J. Appl. Phys. **92**, 2575 (2002).

[35] S. Lany, Phys. Rev. B **78**, 245207 (2008).

[36] H. Peng, D. O. Scanlon, V. Stevanovic, J. Vidal, G. W. Watson, and S. Lany, Phys. Rev. B **88**, 115201 (2013).

[37] V. Stevanovic, S. Lany, X. Zhang, and A. Zunger, Phys. Rev. B **85**, 115104 (2012).

[38] J. Neugebauer and C. Van de Walle, Appl. Phys. Lett. **69**, 503 (1996).

[39] T. Mattila and R. M. Nieminen, Phys. Rev. B **55**, 9571 (1997).

[40] R. Gillen and J. Robertson, J. Phys.: Condens. Matter **25**, 405501 (2013).

[41] M. A. Reshchikov and R. Y. Korotkov, Phys. Rev. B **64**, 115205 (2001).

[42] D. M. Hofmann, D. Kovalev, G. Steude, B. K. Meyer, A. Hoffmann, L. Eckey, R. Heitz, T. Detchprom, H. Amano, and I. Akasaki, Phys. Rev. B **52**, 16702 (1995).

[43] A. F. Wright, J Appl. Phys. **98**, 103531 (2005).

[44] T. Mattila and R. M. Nieminen, Phys. Rev. B **54**, 16676 (1996).

[45] S. Limpijumnong and C. G. Van de Walle, Phys. Rev. B **69**, 035207 (2004).

[46] A. Y. Polyakov, M. Shin, J. A. Freitas, M. Skowronski, D. W. Greve, and R. G. Wilson, J. Appl. Phys. **80**, 6349 (1996).

[47] M. A. Reshchikov, G.-C. Yi, and B. W. Wessels, Phys. Rev. B **59**, 13176 (1999).

[48] D. Huang, F. Yun, P. Visconti, M. A. Reshchikov, D. Wang, H. Morkoç, D. L. Rode, L. A. Farina, C. Kurdak, K. T. Tsen, S. S. Park, and K. Y. Lee, Solid-State Electron. **45**, 711 (2001).

[49] D. C. Look, in *Proceedings of the Materials Research Society Symposium*, edited by Y. Arakawa, A. Rizzi, J. S. Speck, C. M. Wetzel, and E. T. Yu (Materials Research Society, Warrendale, PA, 2003), Vol. 743, p. L10.1.

[50] H. Morkoç, Mater. Sci. Eng. R **33**, 135 (2001).

[51] M. A. Reshchikov, H. Morkoç, S. S. Park, and K. Y. Lee, Appl. Phys. Lett. **78**, 2882 (2001).

[52] T. Ogino and M. Aoki, Jpn. J. Appl. Phys. **19**, 2395 (1980).

[53] M. A. Reshchikov, H. Morkoç, S. S. Park, and K. Y. Lee, in *Proceedings of the Materials Research Society Symposium*, edited by S. F. Chichibu, D. C. Look, J. Neugebauer, J. E. Northrup, and H. Riechert (Materials Research Society, Warrendale, PA, 2002), Vol. 693, p. I619.

[54] K. Saarinen, T. Laine, S. Kuisma, J. Nissilä, P. Hautojärvi, L. Dobrzynski, J. M. Baranowski, K. Pakula, R. Stepniewski,

M. Wojdak, A. Wysmolek, T. Suski, M. Leszszynski, I. Grzegory, and S. Porowski, Phys. Rev. Lett. **79**, 3030 (1997).

[55] F. J. Xu, B. Shen, L. Lu, Z. L. Miao, J. Song, Z. J. Yang, G. Y. Zhang, X. P. Hao, B. Y. Wang, X. Q. Shen, and H. Okumura, J. Appl. Phys. **107**, 023528 (2010).

[56] S. Suihkonen, H. Nykänen, T. Tanikawa, M. Yamaguchi, Y. Honda, and H. Amano, Phys. Status Solidi A **210**, 383 (2013).

[57] A. Uedono, T. Fujishima, Y. Cao, Y. Zhang, N. Yoshihara, S. Ishibashi, M. Sumiya, O. Laboutin, W. Johnson, and T. Palacios, Appl. Phys. Lett. **104**, 082110 (2014).

[58] I.-H. Lee, A. Y. Polyakov, N. B. Smirnov, A. V. Govorkov, A. S. Usikov, H. Helava, Yu. N. Makarov, and S. J. Pearton, J. Appl. Phys. **115**, 223702 (2014).